Galaxy Magnitudes & Colors

- Magnitude for Extended Objects
- Optical & NIR filter systems
- Broad properties of galaxy spectra
  - absorption lines (optical & NIR)
  - emission lines (overview)
- Stellar population synthesis
- Age-Sensitive colors
- Metallicity-Sensitive colors
- Breaking the Age+Metallicity Degeneracy

Standard Photometric Apertures

- Within a fixed angular size (3″ typical)
  - but, fraction of detected flux varies with distance
- Within a limiting isophotal surface brightness
  - but, fraction of detected flux varies with surface brightness
- Within a multiple of an isophotal surface brightness or 1st moment radius [e.g. "Kron (1980) magnitudes" -- "growing" the aperture]
  - better, but still surface brightness dependent
- Within a "metric" aperture [e.g. a fixed number of scale lengths, Petrosian (1976) magnitudes, etc]
  - best, but harder to measure

More specifically, we define the "Petrosian ratio" $\mathcal{R}_P$ at a radius r from the center of an object to be the ratio of the local surface brightness averaged over an annulus at r to the mean surface brightness within r:

$$\mathcal{R}_P(r) \equiv \frac{\int_{\alpha_{lo} r}^{\alpha_{hi} r} dr' 2\pi r' I(r') / [\pi(\alpha_{hi}^2 - \alpha_{lo}^2) r^2]}{\int_0^r dr' 2\pi r' I(r')/(\pi r^2)} , \qquad (1)$$

where $I(r)$ is the azimuthally averaged surface brightness profile and $\alpha_{lo} < 1$, $\alpha_{hi} > 1$ define the annulus. The SDSS has adopted $\alpha_{lo} = 0.8$ and $\alpha_{hi} = 1.25$.

The Petrosian radius r_P is defined as the radius at which $\mathcal{R}_P(r_P)$ equals some specified value $\mathcal{R}_{P,lim}$. The Petrosian flux in any band is then defined as the flux within a certain number N_P of r^* Petrosian radii:

$$F_P \equiv \int_0^{N_P r_P} 2\pi r' \, dr' I(r') . \qquad (2)$$

Thus, the aperture in all bands is set by the profile of the galaxy in r^* alone. The SDSS has selected $\mathcal{R}_{P,lim} = 0.2$ and $N_P = 2$. The aperture $2r_P$ is large enough to contain nearly all of the light for a typical galaxy profile (see below), so even substantial errors in r_P cause only small errors in the Petrosian flux, but small enough that sky noise in F_P is small (typical statistical errors near the flux limit of $r^* = 17.65$ are $< 5\%$). In practice, there are a number of

Based on Petrosian 1976, described in Blanton et al 2001

Petrosian magnitudes partially fix this problem by defining an aperture based on $\Sigma(r)$ that always captures the same fraction of the flux for a given profile (independent of Σ_0 or $r_{1/2}$)

Magnitudes are defined in "systems" relative to some standard which defines m=0

The apparent magnitude m_R of the source is related to its spectral density of flux $f_\nu(\nu)$ (energy per unit time per unit area per unit frequency) by

Hogg et al 2002; astro-ph/0210394

$$m_R = -2.5 \log_{10}\left[\frac{\int \frac{d\nu_o}{\nu_o} f_\nu(\nu_o) R(\nu_o)}{\int \frac{d\nu_o}{\nu_o} g_\nu^R(\nu_o) R(\nu_o)}\right] , \qquad (4)$$

where the integrals are over the observed frequencies ν_o; $g_\nu^R(\nu)$ is the spectral density of flux for the zero-magnitude or "standard" source, which, for Vega-relative magnitudes, is Vega (or perhaps a weighted sum of a certain set of A0 stars), and, for AB magnitudes (Oke & Gunn 1983), is a hypothetical constant source with $g_\nu^{AB}(\nu) = 3631$ Jy (where 1 Jy $= 10^{-26}$ W m^{-2} Hz^{-1} $= 10^{-23}$ erg cm^{-2} s^{-1} Hz^{-1}) at all frequencies ν; and $R(\nu)$ describes the bandpass, as follows:

- Canonical standard is Vega, an A-star (m=0,color=0)
- Negative colors = bluer than A-star
- Other standards possible
  - G-stars = typical of galaxy spectra
  - Flat spectrum = "AB Magnitudes"

Definition of AB Magnitudes: Measured relative to a flat-spectrum source with a constant flux at all frequencies

We refer throughout this paper to AB magnitudes, first defined by Oke & Gunn (1983) to measure the ratio of the number of photons included in the signal of the detector relative to that number for a flat spectrum source with $g(\nu) = 3.631 \times 10^{-20}$ ergs cm^{-2} s^{-1} Hz^{-1}. For a source with a spectrum $f(\nu)$ the AB magnitude should be (for a perfectly calibrated AB system)

$$\begin{aligned} m_{AB} &= -2.41 - 2.5\log_{10}\left[\frac{\int_0^\infty d\lambda\lambda f(\lambda)R(\lambda)}{\int_0^\infty d\lambda\lambda^{-1}R(\lambda)}\right] \\ &= -48.60 - 2.5\log_{10}\left[\frac{\int_0^\infty d\nu\nu^{-1}f(\nu)R(\nu)}{\int_0^\infty d\nu\nu^{-1}R(\nu)}\right], \end{aligned} \tag{2}$$

where $R(\lambda)$ is the fraction of photons entering the Earth's atmosphere which are included in the signal as a function of wavelength (a unitless quantity). Note that $R(\lambda)$ can be defined even for devices which do not count photons directly (such as bolometers). This equation is written such that $f(\lambda)$ is in units of ergs cm^{-2} s^{-1} Å^{-1} and $f(\nu)$ is in units of ergs cm^{-2} s^{-1} Hz^{-1}, while λ is expressed in Å and ν is expressed in Hz. The normalizations defined here mean that an object with $f(\nu) = g(\nu) = 3631$ Jy $= 3.631 \times 10^{-20}$ ergs cm^{-2} s^{-1} Hz^{-1} has all its AB magnitudes equal to zero. The λ^{-1} appears in the integrand of the denominator of the first equation because $g(\lambda) = c/\lambda^2$ for a "flat spectrum" source with $g(\nu) = 1$. The difference in the zeropoints of the two equations simply corresponds to the factor of the speed of light c (expressed in Å s^{-1}) in that expression for $g(\lambda)$.

Blanton et al 2003

Nearly a billion different filter systems are in use (approximately)

Optical filter systems

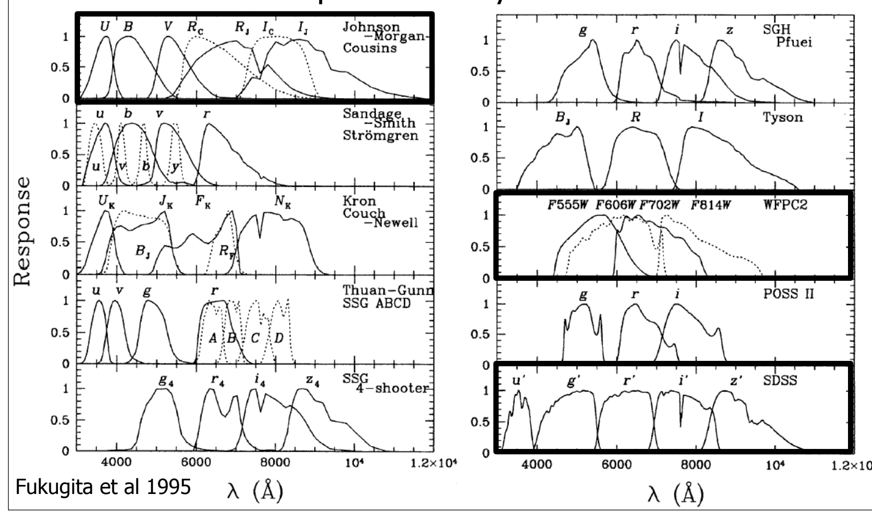

Fukugita et al 1995 λ (Å)

http://www.ipac.caltech.edu/2mass/releases/allsky/doc/sec6_4b.html

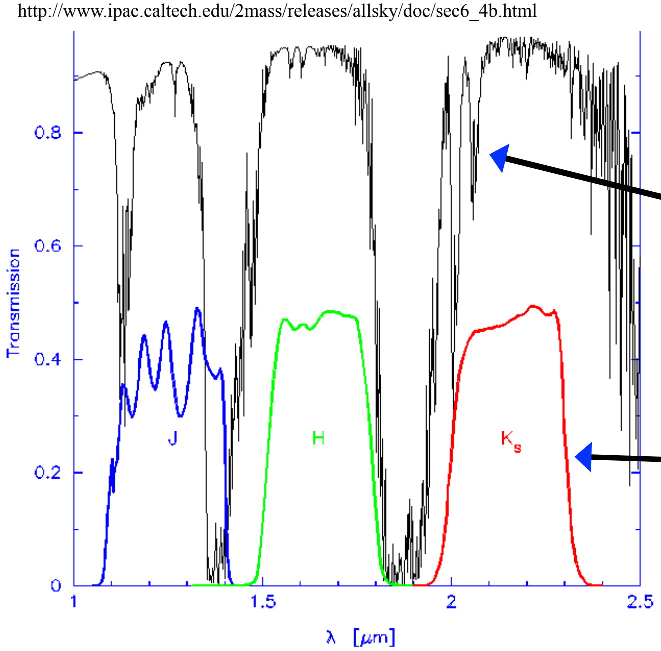

NIR Filters

Atmospheric transmission

2MASS filters

Filters highlight different spectral features

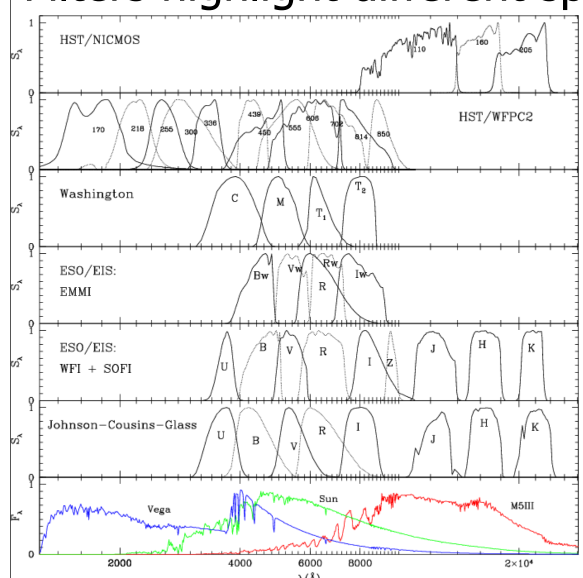

(Girardi, Bertelli, Bressan et al, 2002, A&A, 391, 195)

Very low resolution spectroscopy!

Different filter systems can share same filter names

Must specify name + system

Properties of Optical Filters

Fukugita et al 1995

$$\lambda_{\rm eff} = \frac{\int d\lambda \lambda R(\lambda)}{\int d\lambda R(\lambda)},$$

$$f_\lambda^{\rm eff}(\alpha\ {\rm Lyr}) = \frac{\int d\lambda f_\lambda(\alpha\ {\rm Lyr}) R(\lambda)}{\int d\lambda R(\lambda)},$$

$$\lambda_{\rm eff}(\alpha\ {\rm Lyr}) = \frac{\int d\lambda \lambda f_\lambda(\alpha\ {\rm Lyr}) R(\lambda)}{\int d\lambda f_\lambda(\alpha\ {\rm Lyr}) R(\lambda)},$$

Characteristics of Photometric Bands

bandpass system	band	ref[a]	$\lambda_{\rm eff}$ (Å)	FWHM (Å)	$\lambda_{\rm eff}^{\rm Vega}$ (Å)	$f_{\lambda,{\rm eff}}^{\rm Vega}$ ($\times10^{-9}$cgs/Å)	$c(\nu_{\rm eff}^{\rm Vega})^{-1}$ (Å)	$f_{\nu,{\rm eff}}^{\rm Vega}$ ($\times10^{-20}$cgs/Hz)
Johnson-Morgan	U_3	Buser 78	3652	526	3709	4.28	3617	1.89
	B_2	AS69	4448	1008	4393	6.19	4363	4.02
	V	AS69	5505	827	5439	3.60	5437	3.59
Cousins	R_C	Bessell 90	6588	1568	6410	2.15	6415	3.02
	I_C	Bessell 90	8060	1542	7977	1.11	7980	2.38
Johnson	R_J		6930	2096	6688	1.87	6693	2.89
	I_J		8785	1706	8571	0.912	8545	2.28
Sandage-Smith	u		3647	595	3710	4.30	3610	1.89
	b		4466	1028	4407	6.10	4369	3.97
	v		5423	823	5368	3.75	5365	3.64
	r		6712	969	6628	1.96	6629	2.90
Strömgren	u	Olson74	3465	363	3496	3.24	3452	1.31
	v	Matsu69	4109	197	4119	7.21	4103	4.12
	b	Olson74	4668	176	4666	5.68	4663	4.15
	y	Olson74	5459	244	5455	3.62	5453	3.60
Kron	U_K	Koo 85	3656	556	3737	4.32	3617	1.93
	J_K		4625	1550	4537	5.54	4467	3.82
	F_K		6168	1330	5978	2.64	5982	3.25
	N_K		7953	1786	7838	1.17	7842	2.44
Couch-Newell	B_J		4604	1490	4515	5.73	4474	3.95
	R_F		6694	517	6679	1.92	6677	2.86
Thuan-Gunn	u		3536	412	3542	3.33	3519	1.38
	v		3992	469	4013	6.62	3967	3.50
	g		4927	709	4888	4.84	4885	3.89
	r		6538	893	6496	2.09	6498	2.96
Schneider et al. (4-shooter)	g_4		5147	913	5083	4.34	5075	3.78
	r_4		6659	1028	6600	1.99	6599	2.92
	i_4		8056	1604	7942	1.13	7941	2.41
	z_4		9141	1472	9071	0.797	9045	2.20
Schneider et al. (Pfuei)	g		5238	882	5166	4.14	5160	3.74
	r		6677	916	6602	1.98	6603	2.91
	i		7973	1353	7876	1.16	7876	2.43
	z		9133	984	9054	0.798	9029	2.19
Schneider et al. (narrow bands)	A		6401	534	6384	2.19	6388	2.99
	B		6904	450	6899	1.77	6895	2.81
	C		7526	608	7508	1.36	7509	2.56
	D		8087	515	8077	1.08	8075	2.35
Tyson (CCD)	B_J		4614	1215	4562	5.46	4477	3.80
	R		6585	1373	6503	2.08	6504	2.97
	I		8668	1725	8532	0.928	8508	2.28
WFPC2	F555W		5536	1480	5387	3.62	5381	3.60
	F606W		6102	2050	5901	2.73	5900	3.28
	F702W		6979	1957	6826	1.77	6829	2.82
	F814W		8092	1653	7906	1.14	7923	2.43
POSS II	$g_{\rm POSS}$		5154	942	5121	4.25	5113	3.74
	$r_{\rm POSS}$		6696	1050	6632	1.96	6632	2.90
	$i_{\rm POSS}$		7837	1469	7756	1.21	7761	2.46
SDSS	u'		3585	556	3594	3.67	3530	1.54
	g'		4858	1297	4765	5.11	4748	3.93
	r'		6290	1358	6205	2.40	6210	3.12
	i'		7706	1547	7617	1.28	7623	2.51
	z'		9222	1530	9123	0.783	9098	2.19

Note — a) References are given whenever the response functions are taken from those which are different from the original ones. AS69 stands for Azusienis & Straizys 1969, and Matsu69 for Matsushima 1969.

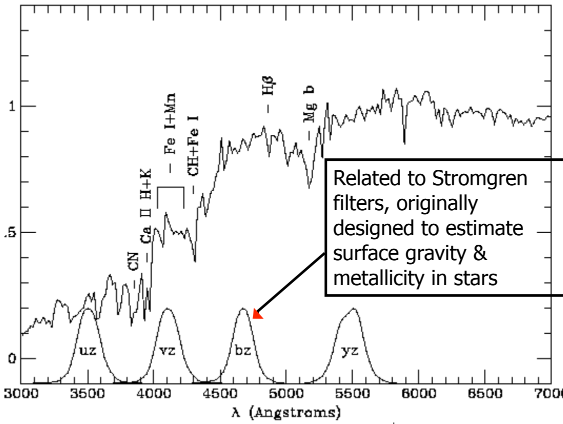

Related to Stromgren filters, originally designed to estimate surface gravity & metallicity in stars

Non-standard "intermediate band" (rather than standard "broad band") filters

Filters isolate physically interesting spectral regions. They are not random!

Wolf et al 2003

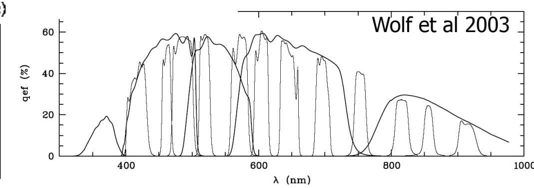

Fig. 1. COMBO-17 filter set: Total system efficiencies are shown in the COMBO-17 passbands, including two telecope mirrors, WFI instrument, CCD detector and average La Silla atmosphere. Combining all observations provides a low-resolution spectrum for all objects in the field. Photometric calibrations of such "multi"-colour datasets are best achieved with spectrophotometric standards inside the target fields.

Colors constrain underlying spectrum

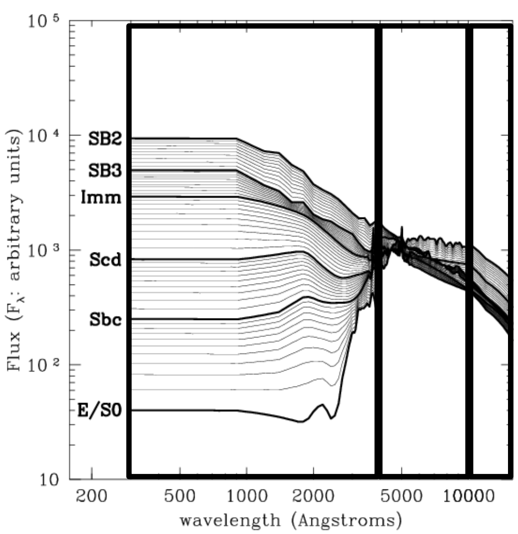

Wider color baseline = more sensitivity

UV, NIR add significant leverage

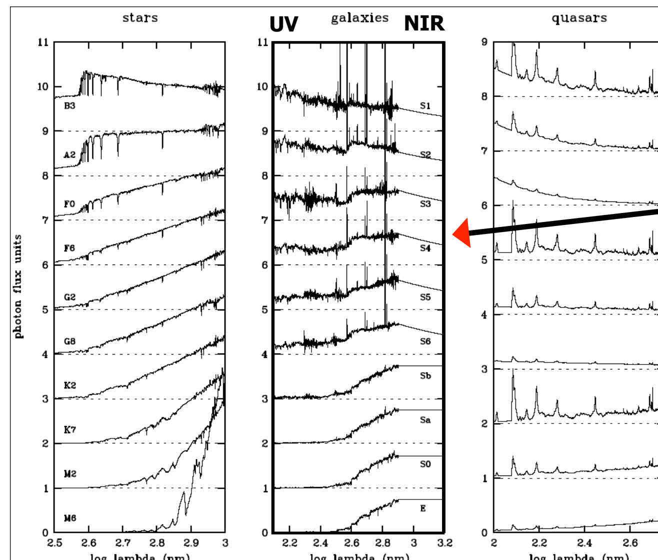

Choose filters that distinguish between spectra

Fig. 1. This diagram shows a few selected spectra from our template libraries. The shown wavelength scale runs from 315 nm to 1000 nm for stars (left), from 125 nm to 1600 nm for galaxies (center) and from 100 nm to 550 nm for quasars (right). The flux is λf_λ in units of photons per nm, time intervall and sensitive area and offset by one unit per step within a class. The flux scale is normalised to unity at 800 nm for stars, arbitrary for galaxies, and normalised to 0.2 at 250 nm for quasars. The stellar templates are taken from Pickles (1998), the galaxy templates from Kinney et al. (1996) and quasar templates are modelled after Francis et al. (1991). The quasar diagram shows nine spectra with three different spectral indices (-2.0, -0.6, +0.8) and three different relative emission-line intensities (0.6, 2.1, 5.7).

Wolf et al 2001

Differences in spectra are apparent even in just the optical

Kennicutt ARAA 1998

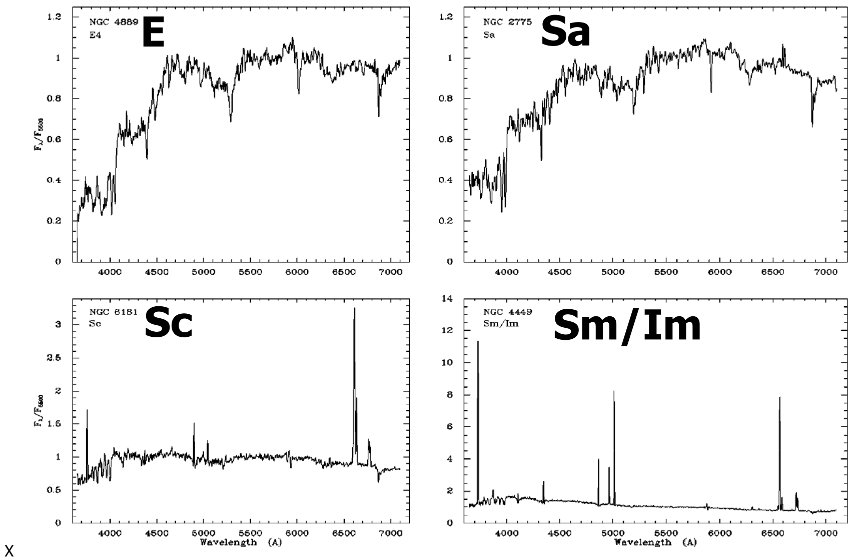

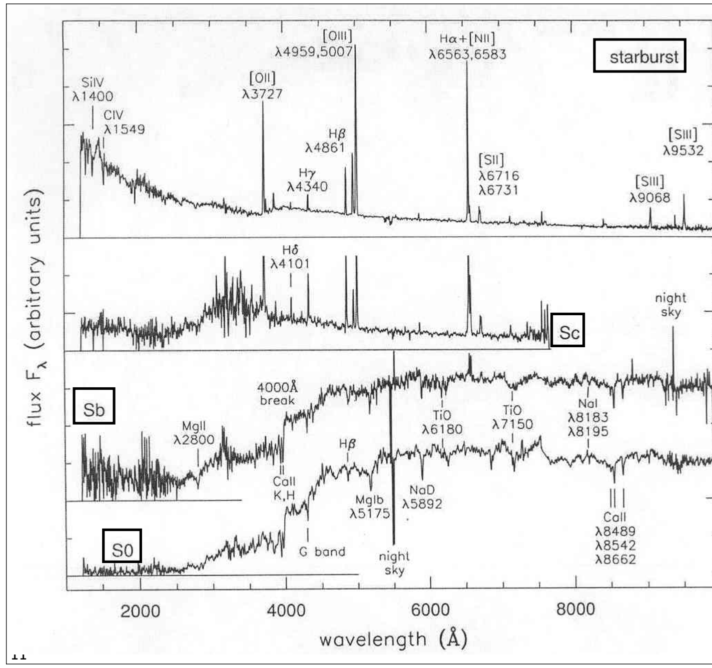

Optical Galaxy Spectra

From Gallagher & Sparke's textbook

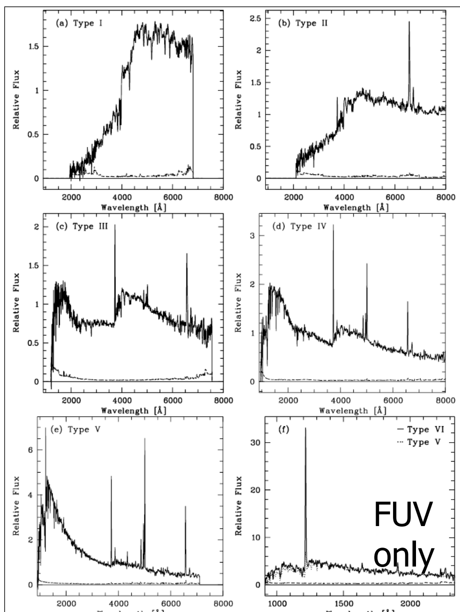

Fig. 3. Empirical templates used for classifying the galaxies of the FDF spectroscopic sample. The noise level is indicated by a dashed line. SEDs I to V are normalised to the same mean flux in the wavelength range 3500 to 4500 Å. SED VI for bright Lyα emitters (panel f)) is adjusted to have the mean flux of SED V between 1400 and 1600 Å. For comparison SED V is overplotted in panel f) (dotted line).

Trends in UV-Optical SEDs

Stronger, bluer UV flux is associated with stronger emission lines (duh!)

Noll et al 2004

Near-IR Spectra: Few features, and few obvious differences among galaxy types

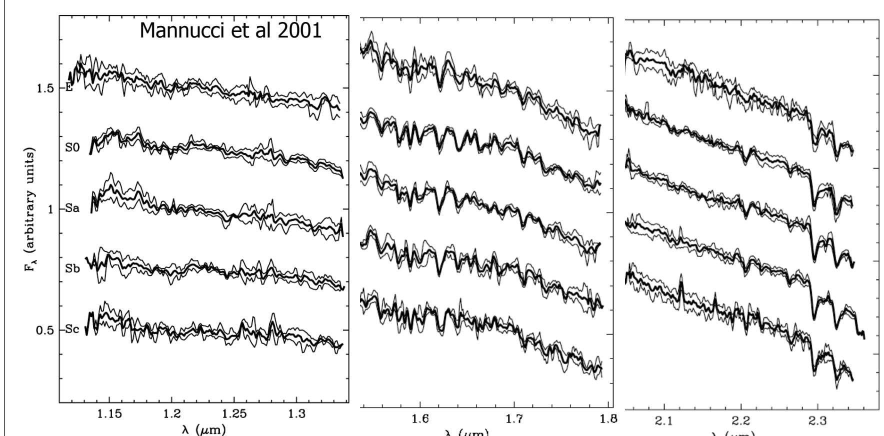

Figure 1. Rest frame average spectra of each class of galaxies in the *J* band. The thick line is the average of the observed spectra, and the thin lines show the ranges within 1 standard deviation. Arbitrary offsets were added to the spectra for clarity.

Figure 2. As Fig. 1, for the *H* band.

Figure 3. As Fig. 1, for the *K* band.

Pretty featureless in the UV too, except for absorption lines due to the ISM (until you get to Lyα)

Index Definitions

Name (2)	Index Bandpass (3)	Pseudocontinua (4)	Units (5)	Measures[a] (6)
CN_1	4142.125–4177.125	4080.125–4117.625 4244.125–4284.125	mag	C, N, (O)
CN_2	4142.125–4177.125	4083.875–4096.375 4244.125–4284.125	mag	C, N, (O)
Ca4227	4222.250–4234.750	4211.000–4219.750 4241.000–4251.000	Å	Ca, (C)
G4300	4281.375–4316.375	4266.375–4282.625 4318.875–4335.125	Å	C, (O)
Fe4383	4369.125–4420.375	4359.125–4370.375 4442.875–4455.375	Å	Fe, C, (Mg)
Ca4455	4452.125–4474.625	4445.875–4454.625 4477.125–4492.125	Å	(Fe), (C), Cr
Fe4531	4514.250–4559.250	4504.250–4514.250 4560.500–4579.250	Å	Ti, (Si)
$C_2$4668	4634.000–4720.250	4611.500–4630.250 4742.750–4756.500	Å	C, (O), (Si)
Hβ	4847.875–4876.625	4827.875–4847.875 4876.625–4891.625	Å	Hβ, (Mg)
Fe5015	4977.750–5054.000	4946.500–4977.750 5054.000–5065.250	Å	(Mg), Ti, Fe
Mg_1	5069.125–5134.125	4895.125–4957.625 5301.125–5366.125	mag	C, Mg, (O), (Fe)
Mg_2	5154.125–5196.625	4895.125–4957.625 5301.125–5366.125	mag	Mg, C, (Fe), (O)
Mgb	5160.125–5192.625	5142.625–5161.375 5191.375–5206.375	Å	Mg, (C), (Cr)
Fe5270	5245.650–5285.650	5233.150–5248.150 5285.650–5318.150	Å	Fe, C, (Mg)
Fe5335	5312.125–5352.125	5304.625–5315.875 5353.375–5363.375	Å	Fe, (C), (Mg), Cr
Fe5406	5387.500–5415.000	5376.250–5387.500 5415.000–5425.000	Å	Fe
Fe5709	5696.625–5720.375	5672.875–5696.625 5722.875–5736.625	Å	(C), Fe
Fe5782	5776.625–5796.625	5765.375–5775.375 5797.875–5811.625	Å	Cr
Na D	5876.875–5909.375	5860.625–5875.625 5922.125–5948.125	Å	Na, C, (Mg)
TiO_1	5936.625–5994.125	5816.625–5849.125 6038.625–6103.625	mag	C
TiO_2	6189.625–6272.125	6066.625–6141.625 6372.625–6415.125	mag	C, V, Sc

"Lick Indices":

Characterize strength of optical absorption features

Age & Metallicity Sensitive

Note that the name sometimes has no connection to what elements are

Trager et al 1998

Table 3. Feature identifications.

λ (μm)	Main contribution	Other species
1.529	OH	CN,TiI
1.540	OH	Si I
1.558	^{12}CO	OH
1.577	^{12}CO	Mg I,Fe I
1.589	Si I	OH
1.598	^{12}CO	Si I,^{13}CO
1.606	OH	
1.619	^{12}CO	OH,Ca I
1.640	^{12}CO	Si I,[Fe II]
1.652	^{13}CO	OH
1.661	^{12}CO	OH
1.669	Si I	OH
1.672	Al I	H I,^{12}CO
1.677	Al I	
1.689	OH	H I,CO
1.710	Mg I	CO,OH
1.723	OH	Si I
1.733	Si I	H I
2.067	Fe I	
2.072	Fe I	
2.081	Fe I	Si I
2.107	Mg I	H_2O,Si I
2.117	Al I	H_2,Mg I,Fe I
2.136	Si I	
2.146	Mg I	Na I,Si I,Ca II
2.166	Brγ	VI
2.173	ScI	Fe I
2.179	TiI	Si I,Fe I
2.189	Si I	TiI,Fe I
2.208	Na I	ScI,TiI,VI,Fe I,Si I
2.226	Fe I	ScI,TiI
2.239	Fe I	ScI
2.248	Fe I	VI,TiI
2.263	Ca I	ScI,TiI,Fe I,S I
2.281	MgI	Ca I,Fe I,S I,HF
2.294	^{12}CO	TiI
2.323	^{12}CO	
2.345	^{13}CO	

NIR absorption line IDs

Spectrum dominated by cool stars

Dominated by Molecules and Low Ionization Species

NIR absorption line IDs

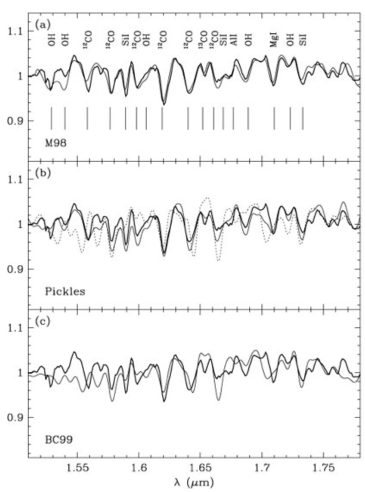

H-band

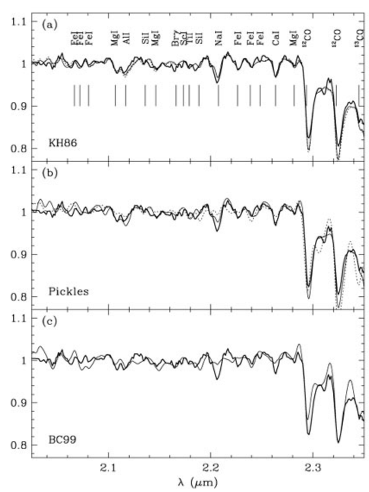

K-band

Mannucci et al

X

Galaxy spectra show emission lines as well: HII regions and/or AGN

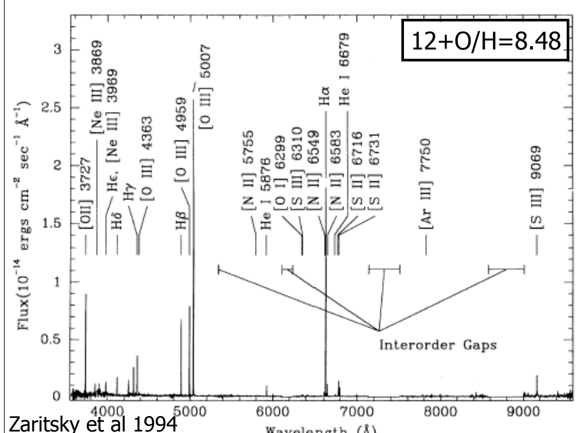

Zaritsky et al 1994

Recombination + Forbidden lines

Photoionization

Shocks

Stars dominate the light in most cases, however

14

For reference: Average galaxy colors measured for different Hubble types

Table 2. Average effective colours of galaxies with $M_V < -21$. For each colour the standard deviation and the number of used objects are also reported.

	$U-B$	$B-V$	$V-R$	$V-I$	$V-K$	$J-H^a$	$H-K^a$
E	0.50	0.99	0.59	1.22	3.30	0.66	0.21
	(0.08)	(0.05)	(0.05)	(0.07)	(0.09)	(0.05)	(0.02)
	323	418	314	221	32	225	225
S0	0.47	0.97	0.58	1.20	3.25	0.66	0.22
	(0.11)	(0.08)	(0.05)	(0.08)	(0.14)	(0.05)	(0.02)
	287	344	227	158	13	235	235
Sa	0.36	0.90	0.58	1.17	3.24	0.67	0.25
	(0.19)	(0.11)	(0.08)	(0.11)	(0.18)	(0.06)	(0.03)
	138	185	73	82	17	105	105
Sb	0.22	0.82	0.57	1.16	3.21	0.66	0.25
	(0.20)	(0.12)	(0.09)	(0.11)	(0.28)	(0.06)	(0.03)
	321	541	156	315	16	93	93
Sc	0.06	0.70	0.52	1.15	3.03	0.66	0.25
	(0.18)	(0.13)	(0.10)	(0.15)	(0.24)	(0.07)	(0.04)
	294	536	133	287	23	46	46
Sd^b	−0.12	0.62	0.47	1.09	2.95	0.65	0.23
	(0.16)	(0.18)	(0.13)	(0.19)	(0.32)	(0.08)	(0.05)
	53	99	25	58	12	26	24
I^c	−0.15	0.51	0.40	1.08	2.35	0.51	0.21
	(0.20)	(0.17)	(0.20)	(0.30)	(0.35)	(0.10)	(0.06)
	102	117	28	35	5	22	20

[a]: The $J-H$ and $H-K$ colours are based also on the results in Fioc & Rocca-Volmerange (1999), where only average quantities are given. In these cases the scatter is not measured but estimated.
[b]: $M_V < -20$.
[c]: No magnitude selection.

Mannucci et al 2001

Continuum = sum of all stellar populations

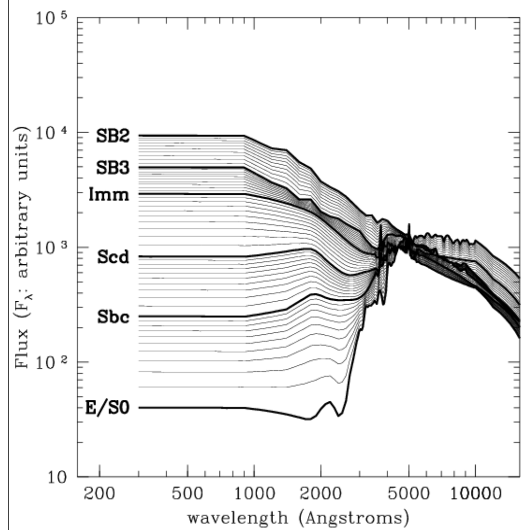

Colors & luminosities are sensitive to the star formation history

http://orca.phys.uvic.ca/~gwyn/pz/specc/

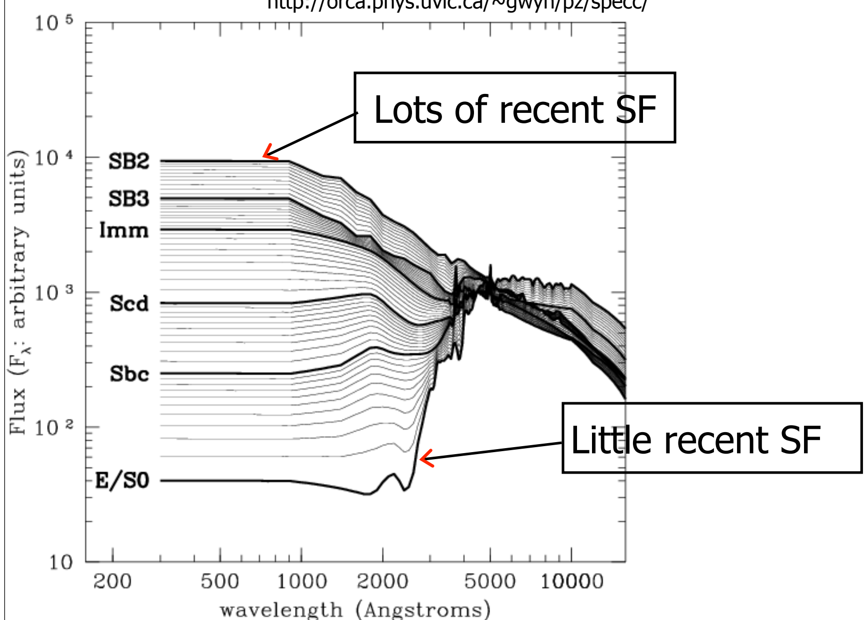

Model the spectrum with "Stellar Population Synthesis"

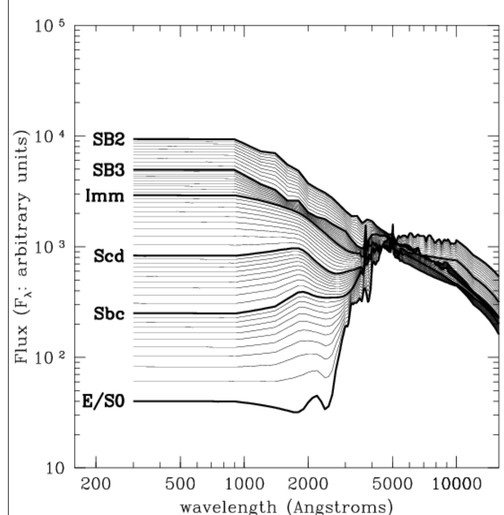

Basis for essentially all estimates of extragalactic physical quantities

(e.g., stellar mass, age, metallicity, extinction, SFRs)

Stellar population synthesis:

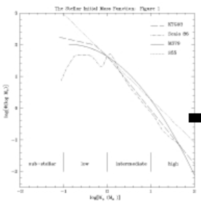

IMF

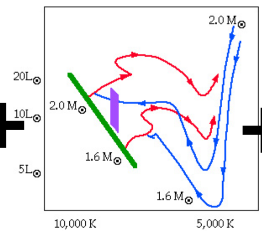

Isochrones & Evolutionary tracks

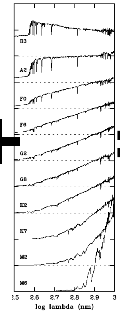

Libraries of Stellar Spectra and/ or Model Atmospheres

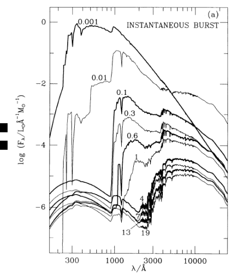

Spectral evolution of a single burst of SF

Arbitrary SFHs can be built up by adding spectra for single bursts at appropriate ages

Instantaneous burst

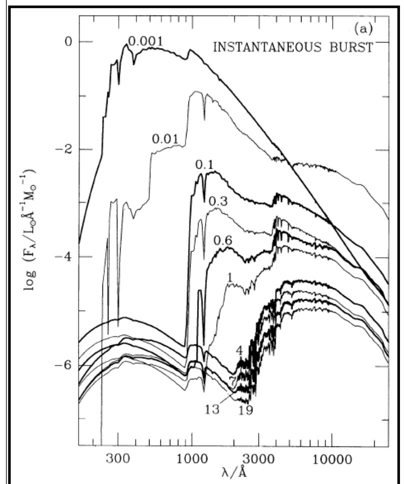

Luminous at early times

Fades and reddens at late times

Little spectral evolution after t>4 Gyr

Young burst can swamp light from old stars

Bruzual & Charlot 1993

FIG. 4.—Spectral evolution of stellar populations with different star formation rates as predicted by the isochrone synthesis model: (a) instantaneous starburst; (b) eq. (2) with $\tau = 3$ Gyr; (c) eq. (2) with $\tau = 7$ Gyr; and (d) constant star formation. In each case, the age (in Gyr) is indicated next to the spectra. Thick lines and thin lines have been used alternatively for clarity. All models have the Salpeter IMF.

Bruzual & Charlot 1993

Instantaneous burst brightens, then fades

Continuous SFR has constant UV spectra, and steady build up of red optical/NIR spectra

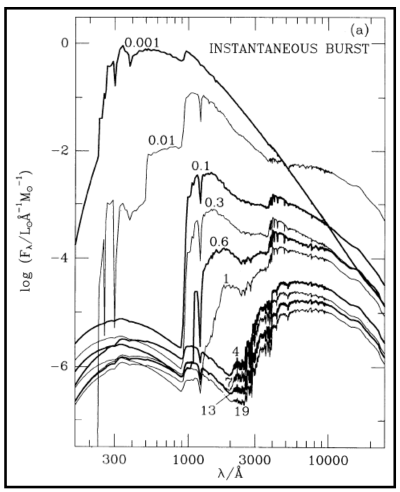

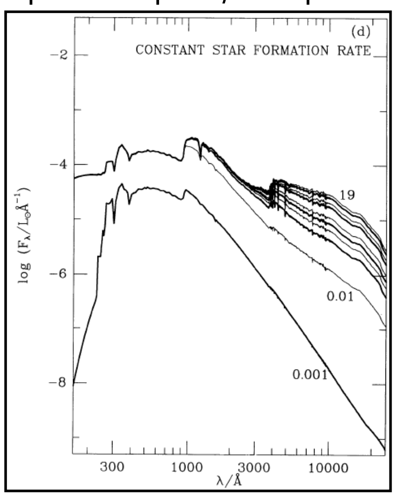

FIG. 4.—Spectral evolution of stellar populations with different star formation rates as predicted by the isochrone synthesis model: (a) instantaneous starburst; (b) eq. (2) with $\tau = 3$ Gyr; (c) eq. (2) with $\tau = 7$ Gyr; and (d) constant star formation. In each case, the age (in Gyr) is indicated next to the spectra. Thick lines and thin lines have been used alternatively for clarity. All models have the Salpeter IMF.

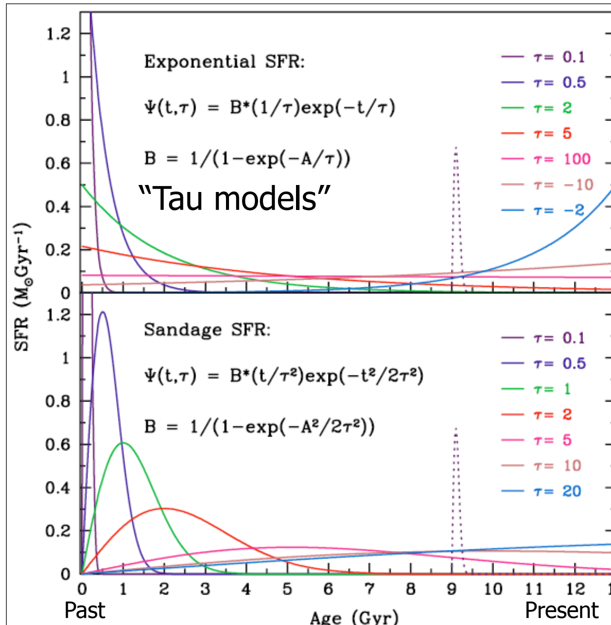

Typical SFHs assumed in stellar population synthesis models

A = age of the galaxy

MacArthur et al 2003

FIG. 4.—Time evolution for the exponential (eq. [6]) (*upper panel*) and Sandage (eq. [8]) (*lower panel*) star formation histories (*solid curves*). The dotted curve is a Sandage-style burst of star formation in which 10% of the total mass of stars are formed. See Fig. 7 for the effect of such a burst on the population model grids.

Spectra for declining exponential SFHs, with timescale τ.

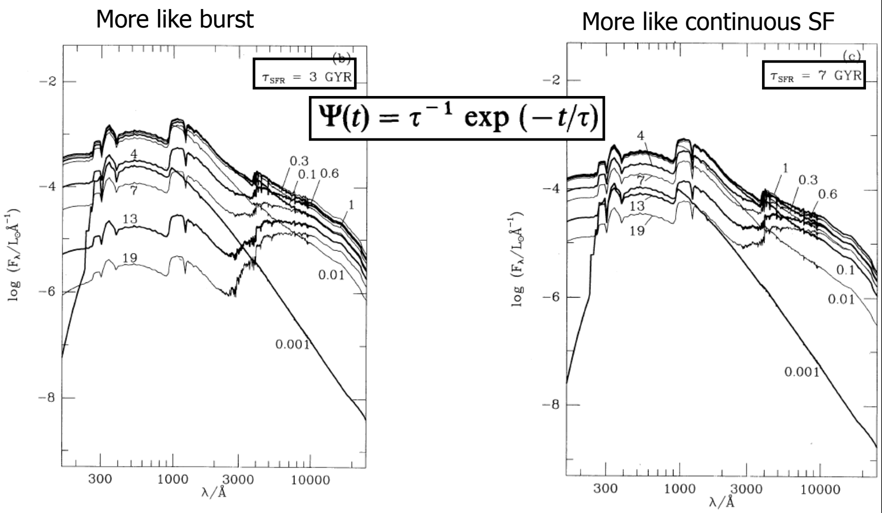

FIG. 4.—Spectral evolution of stellar populations with different star formation rates as predicted by the isochrone synthesis model: (*a*) instantaneous starburst; (*b*) eq. (2) with τ = 3 Gyr; (*c*) eq. (2) with τ = 7 Gyr; and (*d*) constant star formation. In each case, the age (in Gyr) is indicated next to the spectra. Thick lines and thin lines have been used alternatively for clarity. All models have the Salpeter IMF.

SFH affects which stars dominate the spectrum

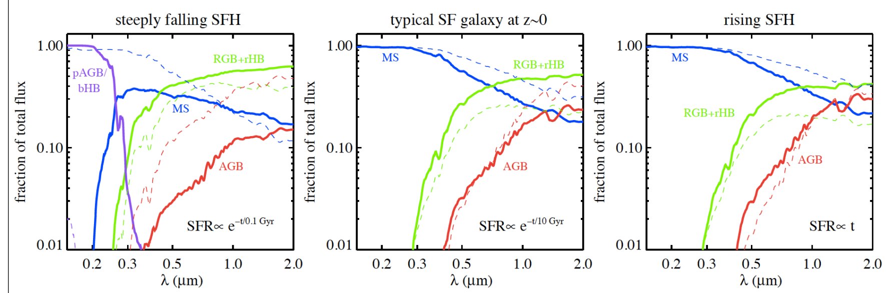

Figure 5:

Top Panels: Fractional contribution to the total flux from stars in various evolutionary phases, for three different SFHs. The left panel is representative of a galaxy that formed nearly all of its stars very rapidly at early times, the middle panel is representative of a typical star-forming galaxy at $z \sim 0$, and the right panel may be representative of the typical galaxy at high redshift. Flux contributions are at 13 Gyr (solid lines) and 1 Gyr (dashed lines) after the commencement of star formation; all models are solar metallicity, dust-free, and are from FSPS (v2.3; Conroy, Gunn & White 2009). Labeled phases include the main sequence (MS), red giant branch (RGB), asymptotic giant branch (AGB, including the TP-AGB), post-AGB (pAGB), and the blue and red horizontal branch (bHB and rHB). Bottom Left Panel: Fractional flux contributions for

 Conroy et al, ARAA 2013

Main Sequence dominates UV/Opt

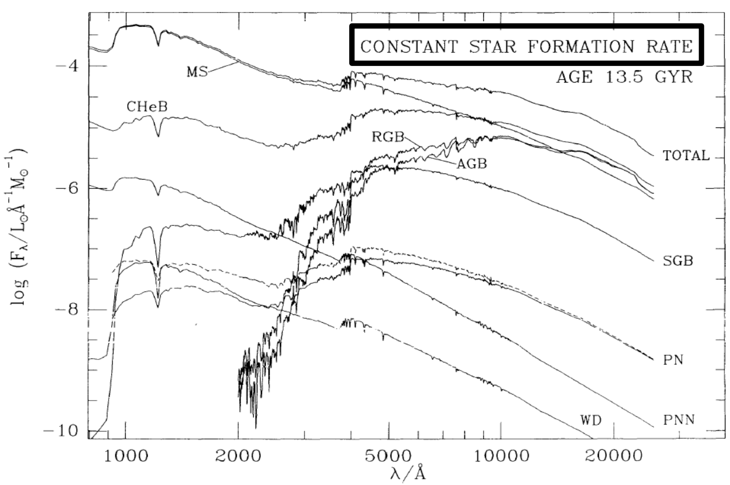

In Figure 9 we indicate the contributions to the total spectral energy distribution of the 1 Gyr burst model, at 13.5 Gyr, of stars in eight groups (the turnoff mass at 13 Gyr is about 0.85 $M_\odot$): main sequence (MS), subgiant branch (SGB), red giant branch (RGB), core He burning (CHeB), planetary nebula (PN), bare PN nucleus (PNN), and white dwarf (WD).

tellar population with constant star formation rate at age 13.5 Gyr

RGB stars dominate the NIR of old galaxies

AGB stars contribute more in NIR at younger ages (high z)

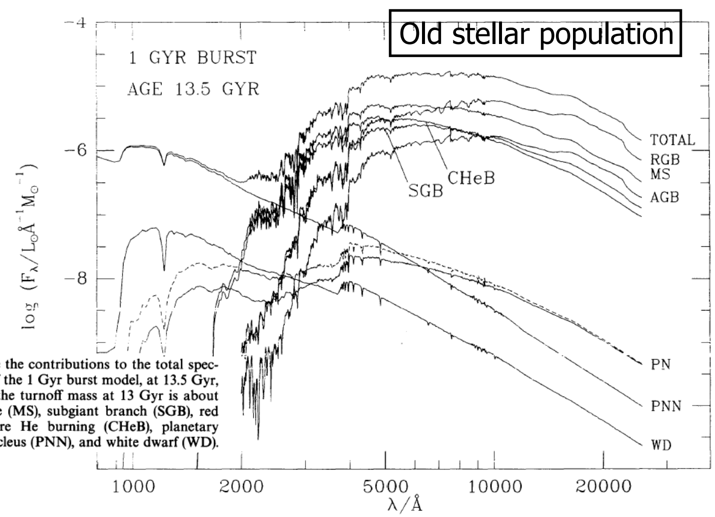

In Figure 9 we indicate the contributions to the total spectral energy distribution of the 1 Gyr burst model, at 13.5 Gyr, of stars in eight groups (the turnoff mass at 13 Gyr is about 0.85 $M_\odot$): main sequence (MS), subgiant branch (SGB), red giant branch (RGB), core He burning (CHeB), planetary nebula (PN), bare PN nucleus (PNN), and white dwarf (WD).

FIG. 9.—Contribution of stars in different groups to the total spectral energy distribution of a 1 Gyr burst population with the Salpeter IMF at age 13.5 Gyr. The acronyms are defined in § 3.5. The dashed line next to the PN contribution corresponds to the case where extinction of the core radiation by the surrounding nebula is ignored. The vertical scale corresponds to a total mass in stars of 1 $M_\odot$.

Stellar population synthesis (SPS):

Compilation: http://www.sedfitting.org/SED08/Models.html

- Many different publicly available codes:
  - FSPS (Conroy)
  - GISSEL (Bruzual & Charlot)
  - PEGASE (Rocca-Volmerange)
  - STARBURST99 (Leitherer)
- Various features can be added on:
  - Metallicity evolution
  - Dust
  - Emission lines

Dust + Metallicity

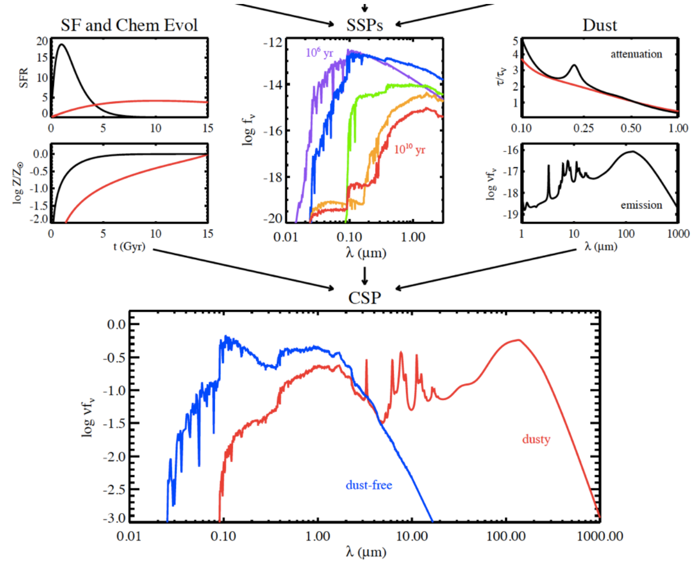

Conroy et al, ARAA 2013

Dust + Metallicity

- FIR gives significant leverage on disentangling dust vs SFR
- But, very model dependent

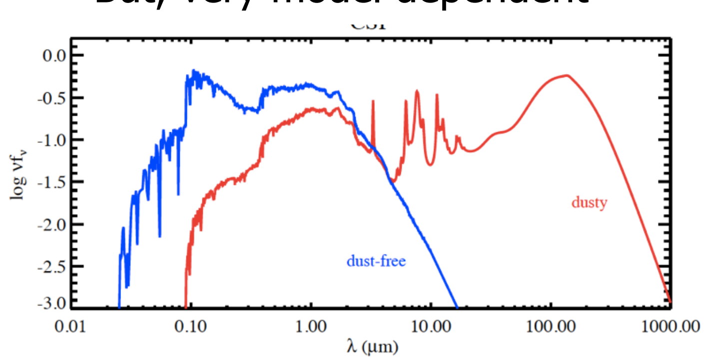

Conroy et al, ARAA 2013

Stellar population synthesis:

- Limitations:
  - Quality of spectral libraries (not so good in NIR or extreme metallicities)
  - Late-stage (post-main sequence) stellar evolution
  - Cool stars

Uncertainties in Ingredients:

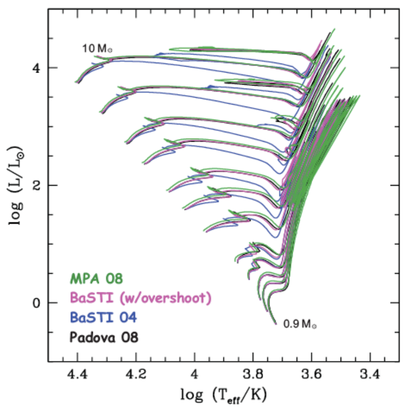

Fig. 1 Evolutionary tracks of solar composition low mass stars (0.9 - 10 $M_\odot$) demonstrating the differences between four different models (as labelled): MPA08 (Weiss and Schlattl 2008), BaSTI04 (with/without overshoot; Pietrinferni et al. 2009), and Padova08 (Marigo and Girardi 2007; Marigo et al. 2008) [Courtesy S. Charlot].

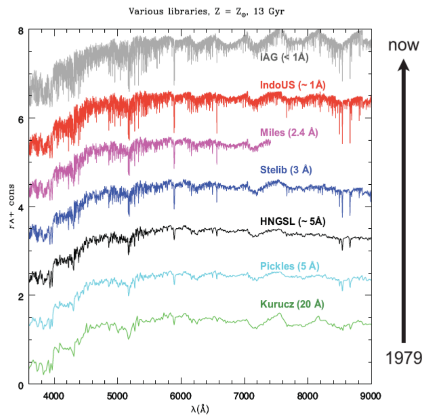

Fig. 2 Optical spectra from both theoretical and empirical stellar libraries (as labelled) demonstrating the improvement of spectral resolution over time with the associated improvement in library size [Courtesy S. Charlot].

See Conroy et al 2009, Conroy & Gunn 2010 for assessment of uncertainties

Nice Review of Synthesis Modeling: Walcher et al 2010

Two basic roles for SPS models

- Predict observable properties given star formation history, metallicity, etc.
- Infer fundamental properties (SFR, stellar mass, etc) from observed spectrum.

The latter can be highly degenerate

However, in the age of widespread spectra + multiwavelength data, using SPS for inference is unavoidable

(and better than most alternatives)

Degeneracies in SPS models

Spectra are "light weighted", favoring young ages

Old SSPs are faint and hard to detect

Complex SFH's bias inference

Higher SNR spectra, wide wavelength coverage all help

Relative measures always better than absolute

Summary: Be cautious if you need a factor of 2 rather than a factor of 10 level of accuracy!